Materials Science and Engineering B 305 (2024) 117401

Contents lists available at ScienceDirect

Materials Science & Engineering B

journal homepage: www.elsevier.com/locate/mseb

Photovoltaic efficacy of CNGS as BSF and second absorber for CIGS thin film solar cells- numerical approach by SCAPS-1D framework

Essaadia Oublal [a,*], Mohamed Al-Hattab [b], Abdelaziz Ait Abdelkadir [a], Mustapha Sahal [a], Naveen Kumar [c]

[a] MESE/Lab. PETI, Ouarzazate Polydisciplinary Faculty, University of Ibnou Zohr, Morocco
[b] LRPSI, Beni Mellal Polydisciplinary Faculty, Sultan My Slimane University, Morocco
[c] Department of Chemistry, Maharshi, Dayanand University, Rohtak 124001, India

ARTICLE INFO

Keywords:
SCAPS-1D
CIGS
CNGS
BSF
Extra absorber

ABSTRACT

Solar cells based on CIGS have outperformed many thin film solar cells using other absorbers. A prospective CIGS active layer-based SC with an ITO/CdS/CIGS/CNGS hetero-structure, with a CdS buffer layer, ITO window layer, and CNGS in dual role: as extra absorber layer, and Back Surface Field (BSF) was suggested in this article. Through the utilization of the unidimensionnal simulation program (SCAPS-1D), the impacts of the absorbers densities of doping and thicknesses, interfacial defects, parasitic resistances, and working temperature on the device have been thoroughly examined. By exploring simulation results, excellent PV metrics, including 1.21 V, 32.25 mA/cm^2, 75.08 %, and 29.39 % for Voc, Jsc, FF, and PCE are provided. The suggested hetero-structure based on CIGS, when simulated, offers a useful technique to create new solar cells with more performance than previously published devices.

1. Introduction

The creation of highly effective PV materials is the main focus of current photovoltaic research. PV cell materials selection is contingent upon several factors, including non-toxicity, band gap energy, financial charges, stability, and simplicity of production. Flexible solar cells can be created using thin-film solar cells, an ideal method that consumes less material than traditional c-Si technology. Based on the Shockley −Queisser limit, a single p-n junction solar cell's potential peak efficiency of 30 % has been calculated. The Shockley-Queisser limit is being approached and attempted to be crossed by the PCE of CIGS-based SCs. Looking to their great efficiency, CIGS TFSCs are a good choice for widely available, commercially viable applications [1–4]. CIGS-based solar cells can be very useful in aerospace applications because of their low volume and weight, excellent temperature reliability, and small size; however, Gallium (Ga) and indium (In), two costly and rare earth elements, are found in CIGS. Photovoltaic (PV) devices may now be mass-produced at a reasonable cost thanks to compounds generated from kesterites like (CZTS), (CZTSe), and (CZTSe). But, these compounds show lower PCE, Random disorder, and widespread CuZn and ZnCu antisite defects, as well as the creation of secondary phases in ZnS, SnS, Cu2S, and SnS2, are some possible causes of the lower PCE of kesterites-based TFSCs [5–8]. In this case, researchers concluded that one effective strategy to lessen these effects is to substitute alternative chemical substances with the same valence for Cu+, Zn2+, and Sn4 + . For example, the optical band gap of the material can be increased by swapping out tin atoms for germanium atoms. Similarly, in CZGS, replacing zinc with nickel results in the compound Cu_2NiGeS_4 (CNGS), which hasn't gotten as much attention in solar cell research [9,10]. CNGS thin layer was deposited for the first time by M. Beraich et al 2020, their study showed the thin film Cu_2NiGeS_4's p-type semiconductor by the Hall Effect measurement, a direct band gap, or band structure, is displayed in the theoretical calculation based on the density functional theory (DFT). The Eg was determined to be between 1.60 and 1.8 eV in both experimental and theoretical work, with a high α (>10^4 cm^{-1}) [11]. The research work mentioned serve as a foundation for the development of this material in the photovoltaic industry. One of the most effective tools for examining the optoelectronic characteristics of solar cell devices is SCAPS-1D, which was developed by Professor Burgelman of Ghent University in Belgium. With the use of this program, material behavior may be evaluated prior to manufacture, which saves money and time in the process of fabricating and characterizing solar cells. In essence, three coupled partial differential equations that express

* Corresponding author.
E-mail address: essaadiaoublal97@gmail.com (E. Oublal).

https://doi.org/10.1016/j.mseb.2024.117401
Received 14 February 2024; Received in revised form 18 April 2024; Accepted 26 April 2024
Available online 2 May 2024

Nomenclature

Symbols

μ_n (cm^2/Vs) Electron mobility
μ_p (cm^2/Vs) Hole mobility
N_D(cm^{-3}) Donor's concentration
N_A(cm^{-3}) Shallow uniform acceptor density
Ve/h(cm/s) Thermal velocity of electron/Hole
Nt (cm^{-3}) Defect density
φ(ev) Contact work function
Se(cm/s) Electrons surface recombination velocity
Sh(cm/s Surface recombination velocity for holes
V_{oc}(V) Open circuit voltage
J_{sc}(mA/cm^2) Short circuit current density
Q_e(%) Quantum efficiency
E_g(eV) Band gap
χ (eV) Electron affinity
ε_r Dielectric permittivity (relative)
N_c (cm^{-3}) CB effective density of states
N_v (cm^{-3}) VB effective density of states
α Absorption coefficient

Abbreviations

CNGS(Cu_2NiGeS_4) Copper Nickel Germanium Sulfur
CdS Cadmium Sulfide
ITO Indium Tin Oxide
CIGS ($CuInGaSe_2$) Copper Indium Gallium selenide
HTL Hole Transport Layer
PCE(η(%)) Power Conversion Efficiency
FF(%) Fill Factor
SC Solar Cell
E_g Band gap energy
ETL Electron Transport Layer

Table 1
Input parameters of used materials.

Parameters	ITO [14]	CdS [15]	CIGS [16]	CNGS [17]
W(μm)	0.05	0.05	Varied	Varied
Eg(eV)	3.6	2.42	1.4	1.8
χ(eV)	4.5	4.5	4.5	4.5
εr(relative)	8.9	9	13.6	6.56
N_c (cm^{-3})	2.2×10^{18}	1.8×10^{19}	2.2×10^{18}	2.58×10^{18}
N_v (cm^{-3})	1.8×10^{19}	2.4×10^{18}	1.8×10^{19}	4.54×10^{18}
μn(cm^2/Vs)	10	350	100	100
μp(cm^2/Vs)	10	50	25	25
N_D(cm^{-3})	10^{21}	10^{17}	0	0
N_A(cm^{-3})	0	0	Varied	Varied
Ve(cm/s)	10^7	10^7	10^7	10^7
Vh(cm/s)	10^7	10^7	10^7	10^7
Nt(cm^{-3})	–	10^{17}	10^{14}	10^{14}
ContactsProperties				
	FrontContact	**BackContact**		
φ(eV)	4.34	6.26		
Se(cm/s)	10^7	10^7		
Sh(cm/s)	10^7	10^7		

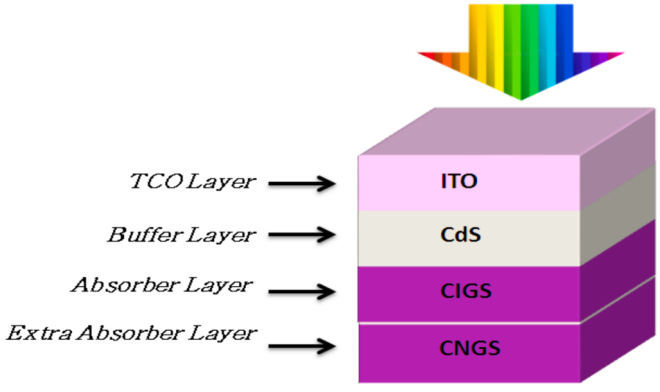

Fig. 1. Solar cell architecture.

the electrostatic potential as well as the concentrations of holes and electrons as functions of position are solved using SCAPS-1D. A comprehensive model for solar cell materials is created via the SCAPS-1D computational framework using the Poisson and the continuity equations for electrons and holes.

In this actual study, we propose making a combination between the famous CIGS compound, and this new derived kesterite, to create a double absorber giving great efficiency in TFSC. The numerical simulation of the new architecture ITO/CdS/CIGS/CNGS, made in this research paper showed a significant improvement in η, 29 % of PCE has been obtained in the final step of numerical simulation, accompanied with excellent PV parameters.

2. Software and solar cell details

- ***SCAPS 1-D***

Here, the SC is numerically modeled and simulated using SCAPS −1D, which has advanced mathematical and physical models. It saves development costs in addition to time. Numerical tools are mostly used to solve problems in real time on virtual platforms. Therefore, before to the real-time manufacture of any device, the majority of design engineers and researchers use simulation. It considers the physical characteristics of the material and mathematical models to provide details about various processes occurring inside the device [12 13]. As can be seen from equations of poisson and continuity (Eq (1) and (2–3))

$$\frac{d}{dx}\left[\varepsilon(x)\frac{d\varphi}{dx}\right] = q\left[p(x) - n(x) + N_d^+ - N_A^- + p_t(x) - n_t(x)\right] \quad (1)$$

where, φ is the electrostatic potential, q is elementary charge, p indicates the density of free holes, and n represents the density of free electrons. N_d^+ and N_A^- are used to refer to the ionized donors and acceptors densities, respectively. Additionally, n_t and p_t denote the densities of trapped electrons and holes, which illustrate the localized charge carriers within the material's defect states. The variable ε denotes the dielectric constant of the medium, which is a fundamental property influencing the electrostatic interactions within the solar cell structure.

$$-\frac{\partial J_n}{\partial x} - U_n + G = \frac{\partial n}{\partial t} \quad (2)$$

$$-\frac{\partial J_p}{\partial x} - U_p + G = \frac{\partial p}{\partial t} \quad (3)$$

J_n and J_p represent the electron and hole current densities, respectively. These densities play a crucial role in understanding how charge carriers move within the solar cell structure. The term $U_{n,\ p}$ refers to the net recombination rate, which encompasses the processes that lead to the annihilation of electron-hole pairs. On the other hand, G represents the electron-hole generation rate.

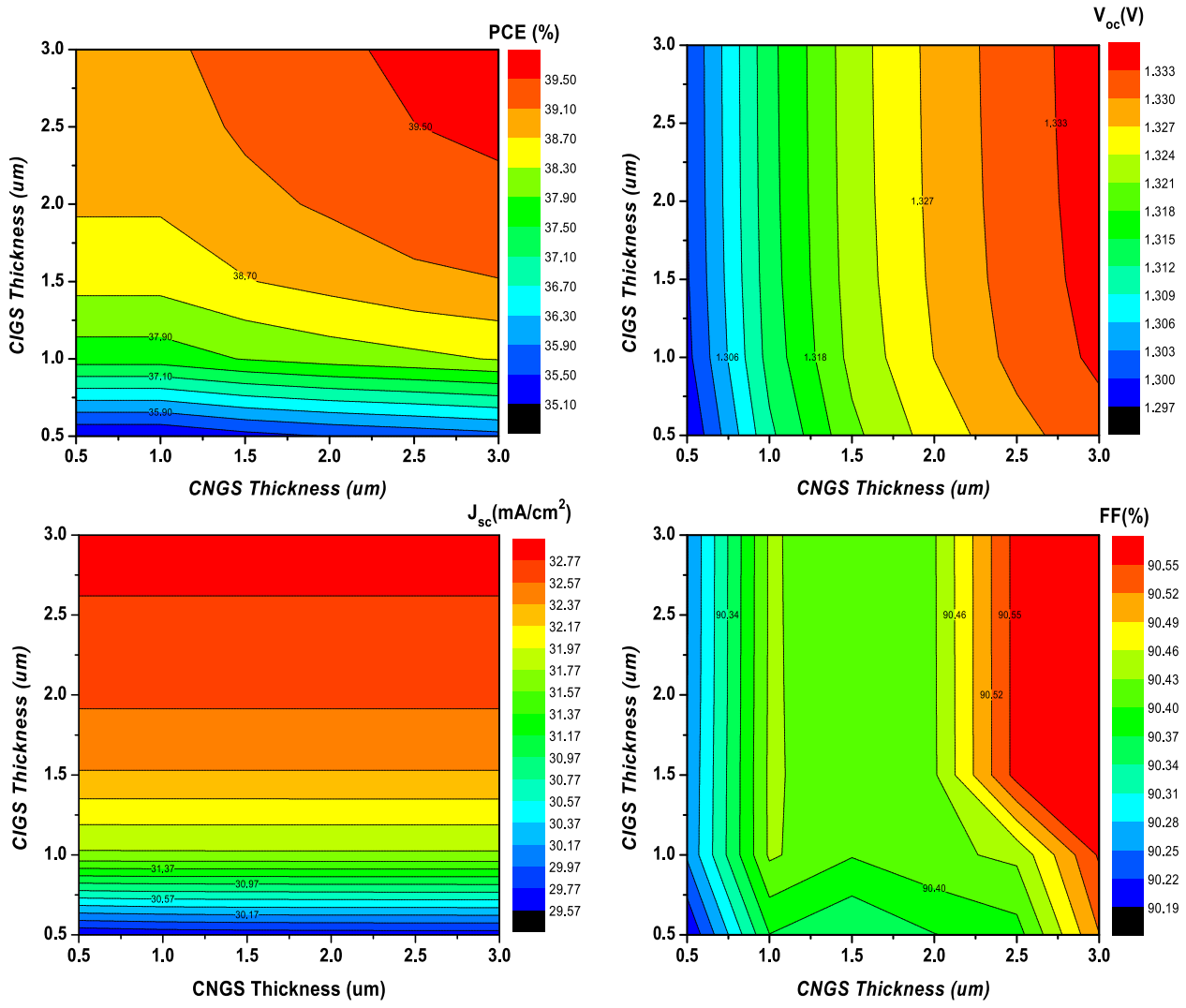

Fig. 2. CIGS and CNGS thicknesses variation.

The physical characteristics of the material were utilized in this modeling as inputs for simulation software. The materials physical properties used for this simulation are depicted in Table 1.

- ***Device structure***

As presented in Fig. 1, the principal materials (CIGS and CNGS) are chosen for the role of absorbing light, where CIGS is the main absorber, and CNGS is the extra absorber. For the buffer layer and the transparent conductor oxide, we opted for the well-known CdS and ITO semiconductors.

3. Results and discussions

- ***Effect of CIGS and CNGS thickness variation***

First, a baseline solar cell architecture comprising p −CNGS/p −CIGS/n −CdS/n −ITO is proposed. The thickness variation is analyzed in order to estimate the overall efficiency of the solar cell at various thickness values ranging from 0.5 to 3 μm, at 0.5 μm increments. As a result, the thickness values are increased in a way that causes an increase for every 0.5 μm value for the solar cell's CNGS and CIGS semiconductor materials separately. Therefore, the scientists employed the contours correlation matrix to show a relationship between the two materials' thickness increment and to clearly show the values of the SC's overall performance at different thickness values for both materials. In Fig. 2 below, four characteristics are highlighted in the contours confusion matrix results: Voc, Jsc, FF, and PCE

As it is clearly noticed on the contours, some photovoltaic outputs are commonly affected by the two absorbers thicknesses, such as PCE and FF, while others are governed by either CNGS or CIGS. V_{oc} is acting more influenced by the extra absorber, which may be explained by its large band gap energy of 1.8 eV [18,19]. However, J_{sc} is depending directly on the CIGS, where every additional increment of thickness increases the current density, because of its lower Eg; CIGS absorbs more light and offers the creation of more electron-hole pairs [20,21].

Because thickness estimate reduces material costs and allows solar cell producers to make the best use of their resources, it is crucial to constructing the most efficient solar cell possible. The presented matrix suggests a thickness value of 1.5 μm for CNGS and also for CIGS, which results in a maximum efficiency for solar cell design.

- ***Effect of CIGS and CNGS acceptors' densities***

The thickness of the solar cell absorbers was optimized by the authors to be 1.5 μm for both semiconductor materials, as determined in the part above. The authors kept the thickness at this value for the study's remaining simulations. Additionally, the contours confusion

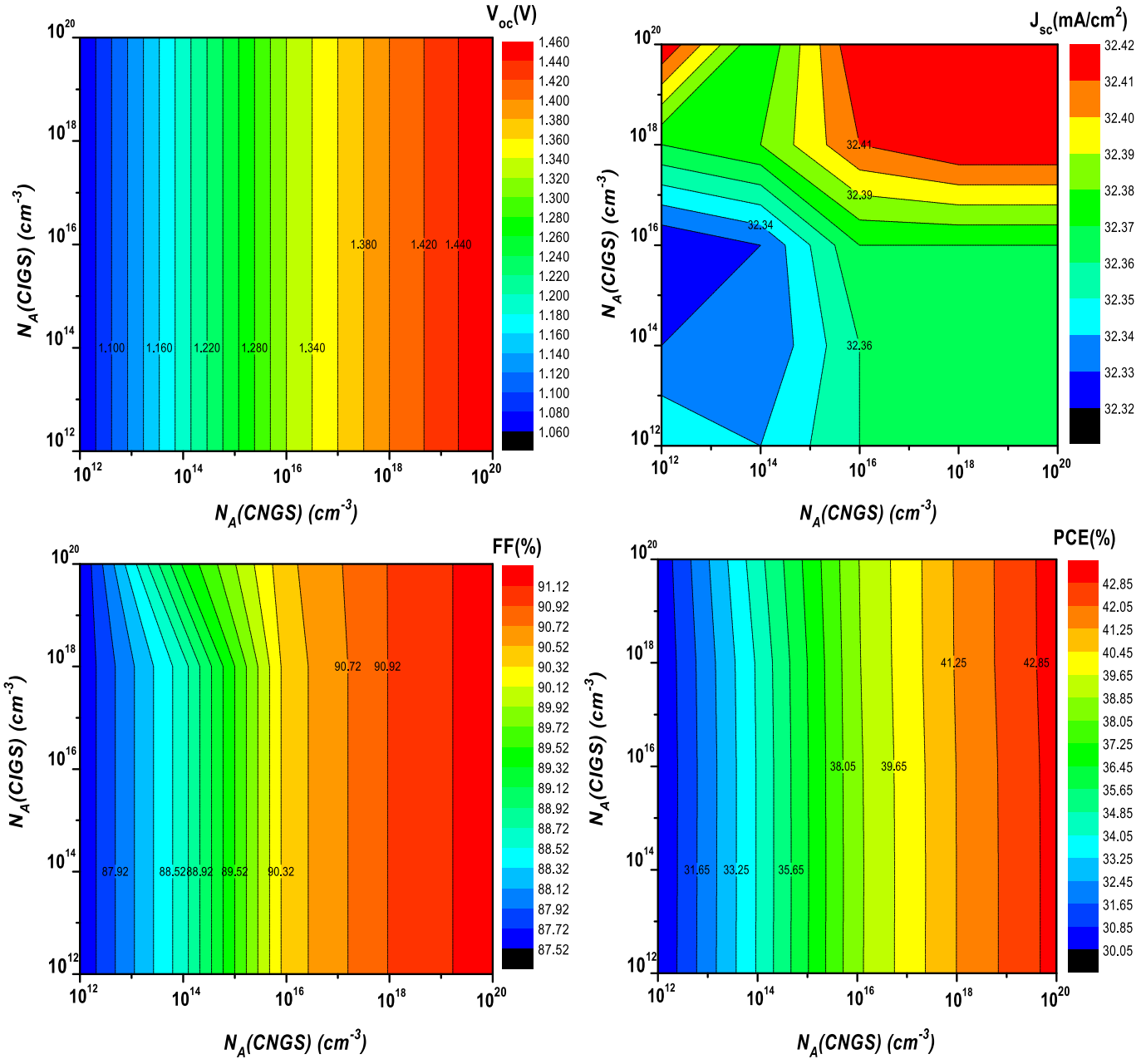

Fig. 3. Effect of N_A densities of CIGS/CNGS on PV metrics.

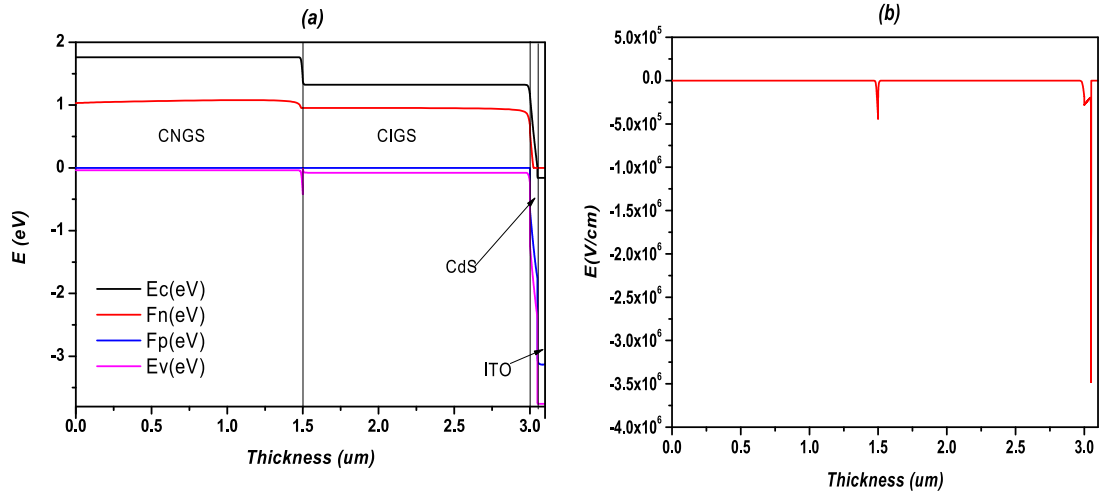

Fig. 4. Band energy alignment (a) and electric field variation (b).

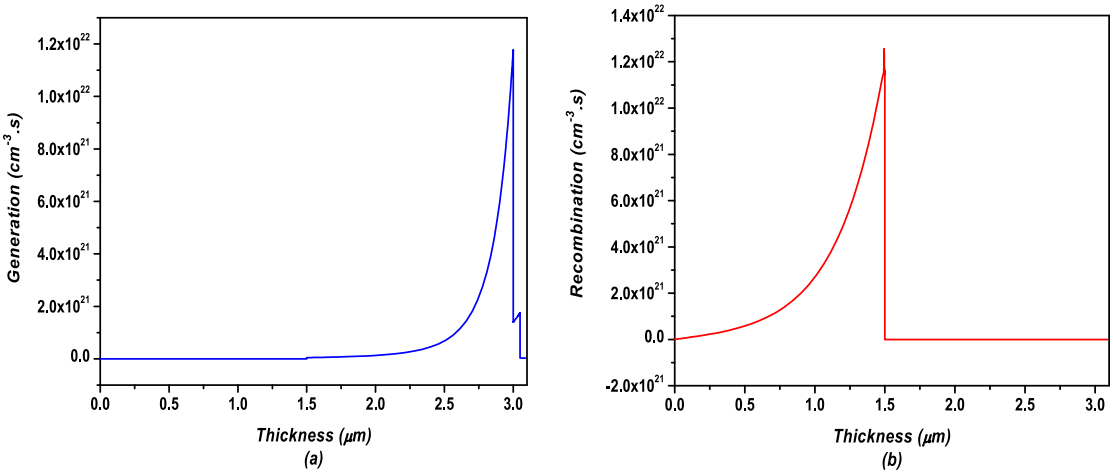

Fig. 5. Generation (a) and recombination (b) present in the structure.

matrix, which provides the N_A density values for both the CNGS and CIGS, are used to evaluate the behavior of the two absorbers against this parameter. Similar to the preceding part, the authors also measured the electrical properties for the crucial doping concentration optimization, such as Efficiency (%) and Fill Factor, among others. As a result, Fig. 3 shows that J_{sc} is slightly affected with these variations; however, the other photovoltaic parameters increase only according to (CNGS) N_A, this increase in CNGS density leads to the creation of a P^+-P junction playing the role of a hole transport layer (HTL), which reduces the recombination of charges and consequently ameliorates the solar cell performance [22,23].

- ***Electric field and energy band diagram***

The energetic alignment between the active material and the charge transport materials has a major impact on the TFSC's performance. The valence band of ETL and absorber should have a considerable offset, but their conduction bands should align with the smallest offset for effective electron separation from the base material. Recombination could result from holes flowing to the ETL if the valence bands are close together. The valence bands of HTL or extra absorber and the main active material should align, whereas their conduction bands should have a significant offset, because electrons are likely to flow to the back of SC if the conduction bands are close together, leading to recombination. Fig. 4 (a) shows the energy band alignment of studied structure, showing that it responds to the conditions mentioned before. Fig. 4 (b) depicts the variation of the electric field in the interfaces present in the structure.

The VBO in the interface CIGS/CNGS is around 0.4 eV, this large and positive offset leads to a negative built-in potential, while the higher electric fields created in CdS/CIGS and ITO/CdS interfaces are due in the first interface to the high VBO, and in the second to both the high VBO and also the large acceptor's density of ITO [24].

- ***Generation and recombination profiles***

As expected and already revealed in previous parts, [25] the principle operations in the solar cell functioning take place in interfaces, Fig. 5 shows that in the P-N junction the separation of charges is the highest, more than 10^{22} cm^{-3} of charges are created. This is due to the high built-in potential presented in the electric field figure. However, the recombination occurs in the interface between the main and the extra absorbers, which may be attributed to the possibility of blocking some electrons and their attendance to the back side of the solar cell.

- ***Interfacial defect densities effect***

Interface defect densities are very important parameters. In this study, as presented in Fig. 6, we analyzed the effect of CNGS/CIGS and CIGS/CdS interfaces defects on the photovoltaic performance of the actual solar cell. Defects concentrations are varied from 10^{10} to 10^{18}

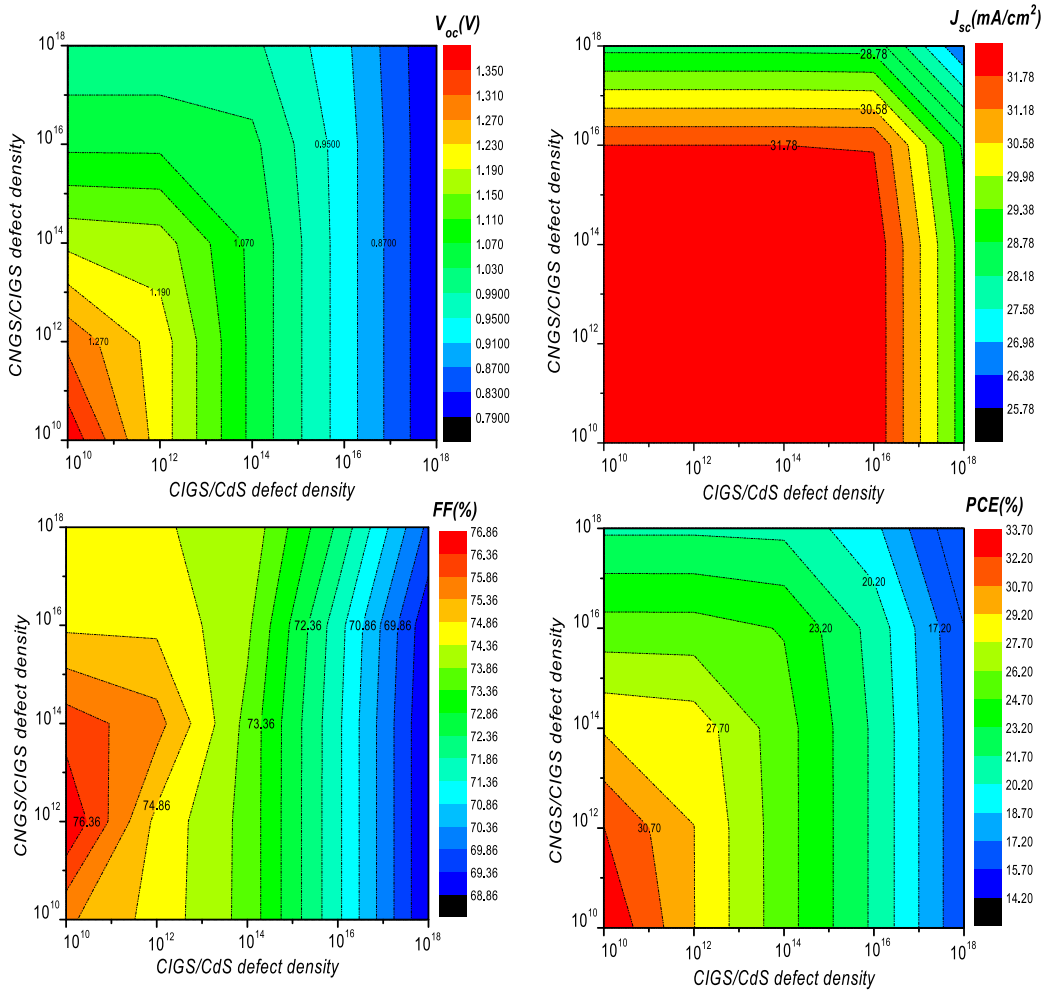

Fig. 6. Impact of interfacial defects.

cm^{-3}, and as we can notice the CNGS/CIGS are more influencing the power conversion efficiency of the cell. In this case we chose 10^{12} for CNGS/CIGS and CIGS/CdS.

■ *R_s and R_{sh} Resistances*

Using the SCAPS-1D simulation tool, the effects of the series and shunt resistances can be investigated. Fig. 7 illustrates the effects of Rs and Rsh on the PV properties of ITO/CdS/CIGS/CNGS heterostructure S.C. Since the Rsh and Rs resistances regulate the J-V shape and slope properties, they have a remarkable impact on SC performance. According to [26], (Rs) is produced by electrical resistance connected to the contacts between the S.C. layers and the front and rear metal contacts, as well as by electrical dissipation occurring in the active layer. The S.C. design has a significant impact on the Rsh since it arises from the charge recombination mechanisms, including leakage current across cell edges. All PV parameters decrease as the R_s values rise, with the exception of J_{sc} which exhibited independent behavior from the R_s. Simultaneously, as the R_{sh} increases, the PCE and FF rise and stabilize at higher values; the V_{oc} is very slightly impacted by the shunt resistance, and the J_{sc} exhibits independent behavior from the R_{sh}.

■ *Working temperature variation effect*

Based on Table 2, we found that the proposed S.C. functions at its best at room temperature. However, any increase in temperature has an impact on all fundamental factors. Furthermore, we observe that Voc, FF, and PCE have significantly decreased, while the J_{sc} has remained constant (showing a minor gain).

Elevated temperatures frequently affect the mobility of charge carriers, electron and hole concentrations, and the material's band gap; all of these variables modify the performance of semiconductors. Additionally, increasing the operating temperature of the solar cells decreases their overall efficiency since it increases the material conductivity through the charge carrier's diffusion with thermally stimulated phonons. With the exception of the J_{sc} at T greater than 300 k, photovoltaic solar cells' performance declined as predicted. This is because the electron-hole pair recombination process accelerates due to the decrease of the gap, increasing the dark current in the S.C. Thus, the increase in the reverse saturation current density is the cause of the observed drop in V_{oc} at high temperatures. As a result, the device performs well when the temperature drops, but the higher working temperature lowers the S.C. PCE [27].

■ *J-V and EQE curves for the studied solar cell*

By contrasting the EQE and J-V characteristics of the SC based on CIGS with and without the addition of the extra absorber layer, and under resistances values of 4 and 800 Ω.cm^2, Fig. 8 effectively displays the influence of the CNGS compound. As can be seen in the pictures, creating a second absorber layer at the back of the cell being studied in this work provides advantages. The photovoltaic properties of the cell under investigation significantly improve with the inclusion of the second material (see Table 3). The addition of a second absorber to the rear

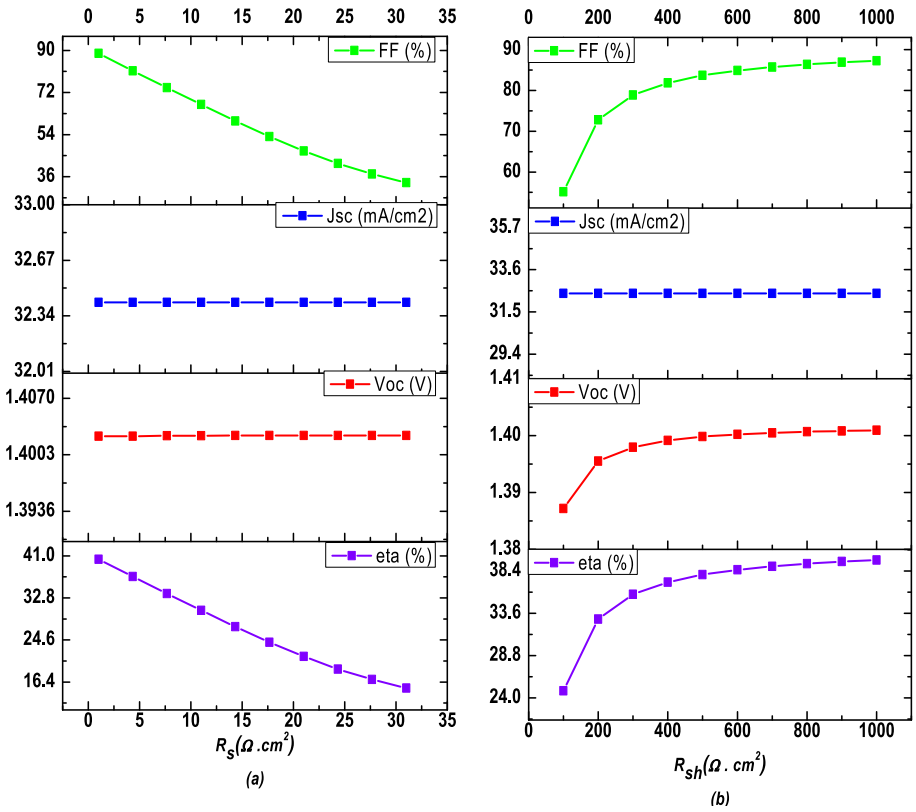

Fig. 7. R_s and R_{sh} variations effect on PV metrics.

Table 2
Influence of working temperature on photovoltaic parameters of proposed SC.

T(K)	$\eta(\%)$	$V_{oc}(V)$	$J_{sc}(mA/cm^2)$	$FF(\%)$
200	47.48	1.56	32.40	93.88
300	41.32	1.40	32.42	90.92
400	34.96	1.23	32.41	87.52
500	28.51	1.05	32.41	83.38

of the ITO/CdS/CIGS structure significantly improves the photovoltaic capabilities of the SC under review [28].

With the addition of the CNGS layer, the V_{oc} significantly increased. [29] The short-circuit current only improved as a result of the extra light absorbed and the newly formed e-h pairs. Due to the extra absorber layer's increased gap energy and potential it is allowed also to function as a back surface field, the quantum efficiency QE curves indicate that the addition of the layer may have decreased the back-loading recombination losses.

4. Conclusion

$CuInGaSe_2$ and Cu_2NiGeS_4, two absorber materials with band gap energies of 1.4 eV and 1.8 eV, respectively, these compounds were the subject of a numerical analysis on a thin film solar cell, as demonstrated by the provided results. As shown in the study, the use of these materials is responsible for investigating the effectiveness of double absorbers in

Table 3
Results of simulation for proposed structures.

Structure	$V_{oc}(V)$	$J_{sc}(mA/cm^2)$	$FF(\%)$	$\eta(\%)$
ITO/CdS/CIGS/CNGS	1.21	32.25	75.08	29.39
ITO/CdS/CIGS	1.01	28.99	76.95	24.78

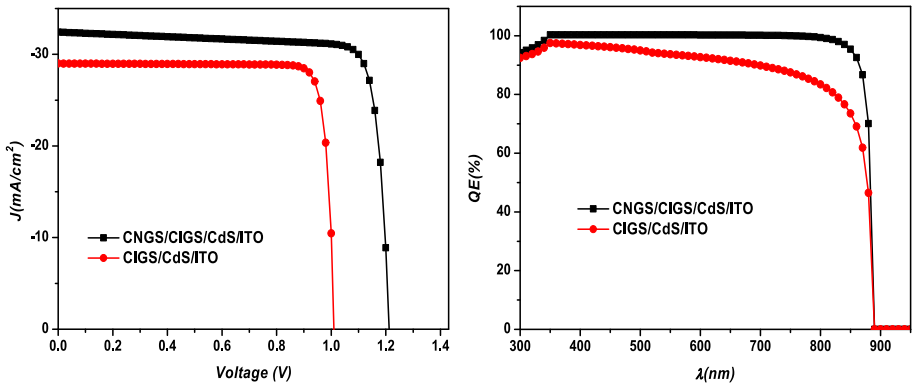

Fig. 8. J-V and EQE curves of ITO/CdS/CIGS/CNGS solar cell.

thin-film solar cells. The simulation tool utilized to get the various outcomes is called SCAPS 1-D, solar cells simulation software, basically working on solving principle equations of physical functioning for solar cells. For ensuring a good PV performance, we first examined the impact of the primary parameters controlling the SC's operation, such as absorber density of doping and thickness. We also looked at the effect of interfacial defects, Rs and Rsh and operating temperature. By displaying the energy band diagram, generation/recombination evolution, and other significant findings, the physical mechanisms were explained. Excellent photovoltaic metrics, including 1.21 V, 32.25 mA/cm^2, 75.08, and 29.39 % for Voc, Jsc, FF, and PCE are provided by the final stage solar cell that was proposed in this research paper.

CRediT authorship contribution statement

Essaadia Oublal: Writing – original draft, Methodology, Investigation, Formal analysis, Data curation, Conceptualization. **Mohamed Al-Hattab:** Writing – review & editing, Visualization, Methodology, Formal analysis, Conceptualization. **Abdelaziz Ait Abdelkadir:** Writing – review & editing, Visualization. **Mustapha Sahal:** Writing – review & editing, Validation, Supervision, Project administration, Investigation, Formal analysis. **Naveen Kumar:** Writing – review & editing, Visualization, Validation.

Declaration of competing interest

The authors declare that they have no known competing financial interests or personal relationships that could have appeared to influence the work reported in this paper.

Data availability

Data will be made available on request.

Acknowledgments

The authors would like to thank Mr. Marc Burgelman for ensuring that *SCAPS −1D* software was available.

References

[1] N. Mufti, T. Amrillah, A. Taufiq, A. Sunaryono, M. Diantoro, H.N. Zulhadjri, Review of CIGS-based solar cells manufacturing by structural engineering, Sol. Energy 207 (2020) 1146–1157, https://doi.org/10.1016/j.solener.2020.07.065.
[2] E. Oublal, A.A. Abdelkadir, M. Sahal, Optimization of a solar cell based on tin sulfide with different BSF materials-numerical approach, in: Veracruz, México, 2023: p. 070004. DOI: 10.1063/5.0171804.
[3] M.K. Hossain, M.S. Uddin, G.F.I. Toki, M.K.A. Mohammed, R. Pandey, J. Madan, M. F. Rahman, M.R. Islam, S. Bhattarai, H. Bencherif, D.P. Samajdar, M. Amami, D. K. Dwivedi, Achieving above 24% efficiency with non-toxic CsSnI $_3$ perovskite solar cells by harnessing the potential of the absorber and charge transport layers, RSC Adv. 13 (2023) 23514–23537, https://doi.org/10.1039/D3RA02910G.
[4] F. Kherrat, L. Dehimi, H. Bencherif, M.M.A. Moon, M.K. Hossain, N.A. Sonmez, T. Ataser, Z. Messai, S. Özçelik, Performance enhancement of eco-friendly Cs3Sb2I9-based perovskite solar cell employing Nb2O5 and CuI as efficient charge transport layers, Micro Nanostruct. 183 (2023) 207676, https://doi.org/10.1016/j.micrna.2023.207676.
[5] M.F. Rahman, N. Mahmud, I. Alam, M.H. Ali, M.M.A. Moon, A. Kuddus, G.F.I. Toki, M.H.K. Rubel, M.A. Al Asad, M.K. Hossain, Design and numerical analysis of CIGS-based solar cell with V2O5 as the BSF layer to enhance photovoltaic performance, AIP Adv. 13 (2023) 045309, https://doi.org/10.1063/5.0138354.
[6] H. Bencherif, Towards a high efficient Cd-free double CZTS layers kesterite solar cell using an optimized interface band alignment, Sol. Energy 238 (2022) 114–125, https://doi.org/10.1016/j.solener.2022.04.040.
[7] A. Thabet, S. Abdelhady, K. Ebnalwaled, A. Ibrahim, Innovative industrial Cu(In, Ga)Se2 thin film solar cell with high characterization using nanoparticles structure, IJEEI 7 (2019) 382–392, https://doi.org/10.11591/ijeei.v7i2.924.
[8] A. Thabet Mohamed, S. Abdelhady, Strategy trends of core/multiple shell for quantum dot-based heterojunction thin film solar cells, Aust. J. Electr. Electron. Eng. 19 (2022) 203–218, https://doi.org/10.1080/1448837X.2021.2023081.
[9] G.E. Delgado, A.V. Sagredo, Synthesis and crystal structure of the quaternary semiconductor Cu2NiGeS4, a new stannite-type compound, Rev. Mex. Fís. 65 (2019) 355–359, https://doi.org/10.31349/RevMexFis.65.355.
[10] J. El Hamdaoui, M. El-Yadri, M. Farkous, M. Kria, M. Courel, M. Ojeda, L.M. Pérez, A. Tiutiunnyk, D. Laroze, E.M. Feddi, Strain Effects on the Electronic and Optical Properties of Kesterite Cu2ZnGeX4 (X = S, Se): First-Principles Study, Nanomaterials 11 (2021) 2692, https://doi.org/10.3390/nano11102692.
[11] M. Beraich, H. Shaili, E. Benhsina, Z. Hafidi, M. Taibi, F. Bentiss, A. Guenbour, A. Bellaouchou, A. Mzerd, A. Zarrouk, M. Fahoume, Experimental and theoretical study of new kesterite Cu2NiGeS4 thin film synthesized via spray ultrasonic technic, Appl. Surf. Sci. 527 (2020) 146800, https://doi.org/10.1016/j.apsusc.2020.146800.
[12] M. Burgelman, P. Nollet, S. Degrave, Modelling polycrystalline semiconductor solar cells, Thin Solid Films 361–362 (2000) 527–532, https://doi.org/10.1016/S0040-6090(99)00825-1.
[13] M. Al-Hattab, E. Oublal, Y. Chrafih, L. Moudou, O. Bajjou, M. Sahal, K. Rahmani, Novel simulation and efficiency enhancement of eco-friendly Cu2FeSnS4/c-silicon tandem solar device, Silicon (2023), https://doi.org/10.1007/s12633-023-02582-5.
[14] E. Oublal, M. Al-Hattab, A. Ait Abdelkadir, M. Sahal, New numerical model for a 2T-tandem solar cell device with narrow band gap SWCNTs reaching efficiency around 35 %, Solar Energy 246 (2022) 57–65, https://doi.org/10.1016/j.solener.2022.09.036.
[15] S. Bhatti, H.U. Manzoor, A. Zoha, R. Ghannam, Achieving 45% efficiency of CIGS/CdS Solar Cell by adding GaAs using optimization techniques, (2023). http://arxiv.org/abs/2309.07551 (accessed October 29, 2023).
[16] A. Ait Abdelkadir, E. Oublal, M. Sahal, B.M. Soucase, A. Kotri, M. Hangoure, N. Kumar, Numerical simulation and optimization of n-Al-ZnO/n-CdS/p-CIGS/p-Si/p-MoOx/Mo tandem solar cell, Silicon 15 (2023) 2125–2135, https://doi.org/10.1007/s12633-022-02144-1.
[17] N. El Ouarie, J. El Hamdaoui, G.S. Sahoo, K.G. Rodriguez-Osorio, M. Courel, M. Zazoui, L.M. Pérez, D. Laroze, E. Feddi, Modeling of highly efficient CNGS based kesterite solar cell: A DFT study along with SCAPS-1D analysis, Sol. Energy 263 (2023) 111929, https://doi.org/10.1016/j.solener.2023.111929.
[18] M. Al-Hattab, Y. Chrafih, E. Oublal, M. Sahal, L. Moudou, O. Bajjou, K. Rahmani, Ab initio investigation for solar technology on the optical and electronic properties of double perovskites Cs 2 AgBiX 6 (X=Cl, Br, I), ECS J. Solid State Sci. Technol. 12 (2023) 094004, https://doi.org/10.1149/2162-8777/acf7ed.
[19] B. Sharma, A.S. Mathur, V.K. Rajput, I.K. Singh, B.P. Singh, Device modeling of non-fullerene organic solar cell by incorporating CuSCN as a hole transport layer using SCAPS, Optik 251 (2022) 168457, https://doi.org/10.1016/j.ijleo.2021.168457.
[20] C.S. Schuster, M. Koc, S. Yerci, Analytic modelling of multi-junction solar cells via multi-diodes, Renew. Energy 184 (2022) 1033–1042, https://doi.org/10.1016/j.renene.2021.11.018.
[21] N. Selmane, A. Cheknane, F. Khemloul, M.H.S. Helal, H.S. Hilal, Cost-saving and performance-enhancement of CuInGaSe solar cells by adding CuZnSnSe as a second absorber, Sol. Energy 234 (2022) 64–80, https://doi.org/10.1016/j.solener.2022.01.072.
[22] E. Oublal, A. Ait Abdelkadir, M. Sahal, High performance of a new solar cell based on carbon nanotubes with CBTS compound as BSF using SCAPS-1D software, J Nanopart Res 24 (2022) 202, https://doi.org/10.1007/s11051-022-05580-7.
[23] M.S. Salem, A. Shaker, M.S. Othman, A.H. Al-Bagawia, M. Fedawy, G.M. Aleid, Numerical analysis and design of high performance HTL-free antimony sulfide solar cells by SCAPS-1D, Opt. Mater. 123 (2022) 111880, https://doi.org/10.1016/j.optmat.2021.111880.
[24] M. Noman, M. Shahzaib, S.T. Jan, S.N. Shah, A.D. Khan, 26.48% efficient and stable FAPbI $_3$ perovskite solar cells employing SrCu $_{2\ O}$ 2 as hole transport layer, RSC Adv. 13 (2023) 1892–1905, https://doi.org/10.1039/D2RA06535E.
[25] M.A. Rahman, Design and simulation of a high-performance Cd-free Cu2SnSe3 solar cells with SnS electron-blocking hole transport layer and TiO2 electron transport layer by SCAPS-1D, SN Appl. Sci. 3 (2021) 253, https://doi.org/10.1007/s42452-021-04267-3.
[26] C. Yadav, S. Kumar, Numerical simulation of novel designed perovskite/silicon heterojunction solar cell, Opt. Mater. 123 (2022) 111847, https://doi.org/10.1016/j.optmat.2021.111847.
[27] E. Oublal, M. Sahal, A.A. Abdelkadir, New theoretical analysis of a novel hetero-junction SnS/CdS solar cell with homo-junction P-P+ in the rear face-numerical approach, Curr. Appl Phys. 39 (2022) 230–238, https://doi.org/10.1016/j.cap.2022.05.008.
[28] A. Bouich, B. Hartiti, S. Ullah, H. Ullah, M.E. Touhami, D.M.F. Santos, B. Mari, Experimental, theoretical, and numerical simulation of the performance of CuInxGa(1–x) S2-based solar cells, Optik 183 (2019) 137–147, https://doi.org/10.1016/j.ijleo.2019.02.067.
[29] N. Guirdjebaye, S. Ouédraogo, A. Teyou Ngoupo, G.L. Mbopda Tcheum, J.M. B. Ndjaka, Junction configurations and their impacts on Cu(In, Ga)Se2 based solar cells performances, Opto-Electron. Rev. 27 (2019) 70–78, https://doi.org/10.1016/j.opelre.2019.02.001.